Limnol. Oceanogr., 46(8), 2001, 1977–1989

Tracking the fate of a high concentration groundwater nitrate plume through a fringing marsh: A combined groundwater tracer and in situ isotope enrichment study

Craig R. Tobias[1]
School of Marine Science, Virginia Institute of Marine Science, College of William and Mary, Gloucester Point, Virginia 23062

Stephen A. Macko
Department of Environmental Sciences, University of Virginia, Charlottesville, Virginia 22930

Iris C. Anderson and Elizabeth A. Canuel
School of Marine Science, Virginia Institute of Marine Science, College of William and Mary, Gloucester Point, Virginia 23062

Judson W. Harvey
U.S. Geological Survey, Reston, Virginia 20192

Abstract

A groundwater plume enriched in $^{15}NO_3^-$ was created upgradient of a mesohaline salt marsh. By measuring the changes in concentration and isotopic enrichment of NO_3^-, N_2O, N_2, NH_4^+, and particulate organic nitrogen (PON) during plume transport through the marsh, in situ rates of dissimilatory nitrate reduction to ammonium (DNRA) and denitrification (DNF) were estimated, as well as N storage in the reduced N pools. For groundwater discharge within the top 10 cm of marsh, NO_3^- removal was 90% complete within the 50 cm of marsh nearest the upland border. The peak NO_3^- loss rate from the plume ranged from 208 to 645 μM d^{-1}. Rates of DNRA (180 μM d^{-1}) and DNF (387–465 μM d^{-1}) processed 30% and 70% of the NO_3^- load, respectively. Terminal N_2O production was approximately equal to N_2 production rates during DNF. Comparison of ^{15}N lost from the $^{15}NO_3^-$ pool and ^{15}N gained in each of the reduced products accounted for only 22% of the reduced ^{15}N, thus indicating N export from the system. Despite high rates of DNRA, the NH_4^+ produced was not a long-term repository for the groundwater-derived N but was instead rapidly immobilized into marsh PON and retained on longer timescales. The small inventory of ^{15}N in the N_2O and N_2 pools relative to DNF rates, coincident with an undersaturation of dissolved argon, indicated that denitrified N was exported to the atmosphere on short timescales. The relative magnitudes of DNF and DNRA in conjunction with the immobilization of NH_4^+ and evasion of N gases dictated the extent of export versus retention of the groundwater NO_3^- load.

Groundwater enriched in nitrogen has been recognized as an important nonpoint nutrient source to nearshore ecosystems, yet little is understood about the behavior of nitrogen (N) at biogeochemically reactive discharge interfaces (Capone and Bautista 1985; Giblin and Gaines 1990; Valiela et al. 1992). One such interface exists at the ecotone between the shallow aquifer and marsh-fringed estuaries.

Because discharge often concentrates at or near the shoreline (Reilly and Goodman 1985; Bokuniewicz 1992), the importance of fringing marshes in attenuating groundwater N loads to adjacent aquatic or marine systems has been argued (Harvey and Odum 1990; Howes et al. 1996). Fringing marshes can function as groundwater nitrogen ''buffers'' only if a significant proportion of the total groundwater discharge contacts the marsh. Although salt balances calculated for tidal creeks draining some New England pocket marshes indicate substantial marsh/groundwater interaction (Valiela and Teal 1979; Howes et al. 1996), discharge through fringing coastal and riparian marshes may constitute only a small percentage of the total groundwater derived nitrate flux to adjacent water masses (Bohlke and Denver 1995; Portnoy et al. 1997; Nowicki et al. 1999). Yet these relatively small fluxes of groundwater and nitrogen (on an estuarine scale) can be large enough to periodically influence the water and nitrogen balance of the fringing marsh ecosystem itself (Tobias et al. 2001*a*,*b*). Therefore, quantification of the mechanisms of nitrogen processing, specifically pathways that result in the retention of or accelerate losses of N, assumes a more critical role in defining the influence of groundwater nitrogen sources on the marsh ecosystem.

[1] Present address: Ecosystems Center, Marine Biological Laboratory, Woods Hole, Massachusetts, 02543. Corresponding author (ctobias@mbl.edu).

Acknowledgments

We express our thanks to J.K. Böhlke, Tom Juster, David Fugate, David Miller, Scott Neubauer, Chris Buzzelli, Tim Dellapena, Betty Neikirk, Peter Raymond, and Matt Church for their assistance in the field and laboratory. We extend further appreciation to Bruce Peterson, Joe Vallino, and two anonymous reviewers for their thoughtful comments. This work was supported by grants from the National Science Foundation (DEB-9120183, DEB-9411974, DEB-9520819, and DEB-9815598), USDA Forest Service (PSW-97-0036CA), and the generosity of Chuck Rafkind at the Colonial National Historical Park. This is VIMS contribution #2409.

Nitrate is the dominant species of dissolved inorganic nitrogen (DIN) in most shallow, aerobic, aquifers (Kraynov et al. 1992; Fetter 1993) and is the most frequently encountered form of anthropogenically enriched DIN discharging from shallow aquifers in the coastal zone (Valiela and Teal 1979; Reay et al. 1993; Portnoy et al. 1997). Marsh sediments with high organic carbon and low redox potential typically demonstrate high rates of potential nitrate reduction. In many wetland studies, denitrification has been considered to be solely responsible for observed nitrate disappearance in sediments in the absence of direct denitrification (DNF) measurements (Xue et al. 1999). Although DNF has figured prominently in the N budget of some New England marshes subject to large groundwater nitrate fluxes, most efforts to study nitrate reduction in marsh or subtidal sediments have not considered alternate nitrate reduction pathways (Valiela and Teal 1979; Koike and Sorenson 1988; Howes et. al 1996).

Dissimilatory nitrate reduction to ammonium (DNRA) may constitute a greater proportion of total NO_3^- reduction in sediments that contain high electron donor : electron acceptor ratios (i.e., DOC: NO_3^-; Tiedje 1988). Laboratory and microcosm incubations have demonstrated that the DNRA contribution to total nitrate reduction appears to be small in freshwater systems but comparable to DNF rates in some salt marsh and anoxic marine sediments (Koike and Hattori 1978; King and Nedwell 1985; Bowden 1986). The rapid biotic and abiotic immobilization of NH_4^+ found in wetland sediments may serve as a link between DNRA and N storage in the sediment particulate organic nitrogen (PON) pool (Smith et al. 1982; Bowden 1986; White and Howes 1994; Anderson et al. 1997). Unlike the gaseous products of denitrification (N_2O and N_2), which may be subject to evasion on relatively short timescales, nitrogen in the PON detrital fraction is prone to more extensive cycling within the sediments and tends to be sequestered on the timescale of years (White and Howes 1994). Therefore, we suggest that the specific pathway of nitrate reduction may dictate the extent of export versus retention of this allochthonous nitrogen source within the ecosystem.

Herein we describe the relative importance of denitrification and nitrate reduction to ammonium with respect to the total consumption of groundwater nitrate during discharge into a mesohaline fringing marsh. In this advection-dominated discharge zone, traditional techniques used to measure N cycling processes, which require the isolation of sediments into cores or slurries, were avoided (Koike and Sorenson 1988; Knowles 1990). Instead, we chose a relatively novel approach that combined a conservative groundwater tracer (bromide) with an in situ ^{15}N-NO_3^- enrichment, to track in situ marsh processing of high NO_3^- concentration groundwater loads. The technique of using an in situ ^{15}N release within advection-dominated systems has been used in streams and small estuaries to elucidate DIN dynamics and trophic N transfer (Peterson et al. 1997; Holmes et al. 2000; Hughes et al. 2000; Tank et al. 2000). To our knowledge, this approach has not been combined with a natural gradient groundwater tracer study within a marsh discharge environment to provide a comprehensive accounting of nitrate fate and transport.

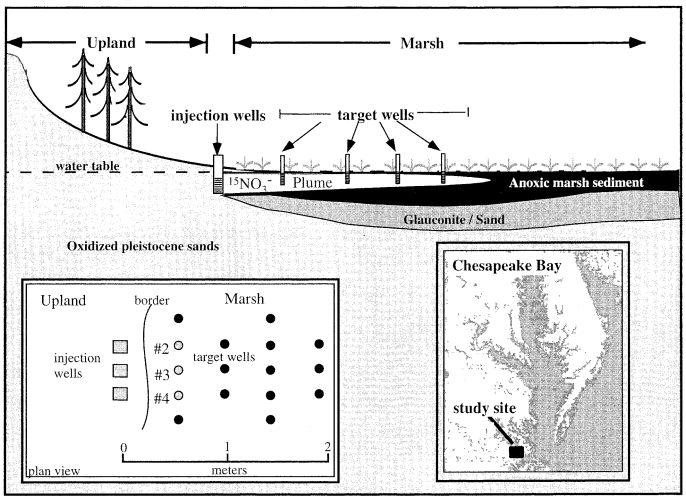

Fig. 1. Site location and site cross section. The target wells used in the mass balance calculation are identified as 2, 3, and 4 in the plan view of the study site. The well field is located 25 m from the marsh-estuary shoreline.

Site description and methods

The Ringfield marsh study site is located in the Colonial National Historical Park (37°16′42″N, 76°35′16″W) on the Ringfield Peninsula near the confluence of King Creek and the York River in southeastern Virginia (Fig. 1). The steep (1 : 1) forested upland slope transitions into a 25-m wide wetland composed of a mixed community of *Spartina cynosuroides* and *Spartina alterniflora* (short form). Marsh stratigraphy consists of the upper 30–80 cm of anoxic marsh sediment underlain by a semicontinuous layer (10–20 cm thick) of lower permeability glauconitic silty sand. Below 150–200 cm, the glauconitic deposits grade into cleaner oxidized iron-rich sands and shell hash of pre-Holocene origin. The site receives maximal groundwater discharge from January through July and little to no discharge from August through November (Tobias et al. 2001*a*).

Tracer release—To simulate high groundwater NO_3^- loads, a concentrated NO_3^- groundwater plume enriched in ^{15}N-NO_3^- and a conservative tracer (Br^-) was created in the shallow aquifer at the border between the upland and the marsh. As the plume discharged into the shallow subsurface of the marsh, the dissolved concentrations and the ^{15}N isotopic enrichments of NO_3^-, NH_4^+, N_2O, and N_2 were measured from wells located in the marsh. Nitrogen incorporated into the sediments (PON) was measured in cores taken before the injection and at the end of the study.

The injectate of $K^{15}NO_3^-$ and KBr was prepared on site by use of groundwater pumped from the injection wells. The final target injectate concentrations for N-NO_3^- and Br^- was 0.12 and 1.0 molar, respectively. The target ^{15}N enrichment was 7600‰–7800‰, and a total of 5 liters of injectate was released into each of the three injection wells. To release the injectate, injection wells were first pumped dry after insertion of a PVC liner, the well volume (now dry) was filled with injectate, and the liner removed. This single slug was

followed by a constant drip at a rate of ~150 ml hr^{-1} for 33 h. The injectate was kept on ice during the drip, and an ultra-high-purity He headspace in the injection reservoir was maintained to prevent atmospheric oxidation of the suboxic (2–3 mg L^{-1} O_2) injectate during the release. The injection and target wells were screened from 5 to 45 cm below the marsh surface, although previous observations during well installations indicated that primary source of water in the marsh wells was from the more hydraulically conductive upper 10 cm of the marsh rhizoshpere. Wells were sealed to the atmosphere and sampled for 100 d postinjection. Wells were purged of three well volumes, or to dryness, under a He headspace and allowed to recharge while venting the headspace through a water trap prior to sampling.

Characterization of bromide and nitrogen pools—The Br^- concentrations in water collected from the target wells were measured in the laboratory by use of an Orion 94–35 Br^--specific electrode after temperature equilibration. All DIN samples were filtered (0.2 μm) in the field. NH_4^+ concentrations were determined by the phenol-hypochlorite method (Solorzano 1969). NO_3^- and NO_2^- concentrations were determined spectrophotometrically with and without cadmium reduction, respectively, by use of an Alpkem autoanalyzer (Alpkem 1992). Isolation of NH_4^+ and NO_3^- for determination of ^{15}N isotopic enrichment followed the diffusion method outlined by Brooks et al. (1989). Recovery of DIN standards by diffusion was >90%. Isotopic analysis of ^{15}N-NH_4^+ was performed at the University of Virginia (UVA) Stable Isotope Facility on a VG Optima isotope ratio mass spectrometer (IRMS) coupled to a C : H : N elemental analyzer. ^{15}N-NO_3^- was analyzed at the University of California, Davis (UCD) Stable Isotope facility. Water samples for N_2O analysis were collected and equilibrated in the field with an equal volume He headspace in a sealed syringe by shaking vigorously for 1 min. After equilibration, headspace was transferred to a gas-tight syringe and analyzed by use of a Shimadzu GC-8 gas chromatograph equipped with a poropak Q column and an electron capture detector. Total dissolved N_2O was determined after correction of headspace concentrations by use of the Ostwald coefficient (Weiss and Price 1980). The remaining headspace sample was transferred into pre-evacuated ''Exetainers'' (Europa Scientific Inc.) and analyzed for ^{15}N-N_2O at UCD.

Samples for dissolved N_2, Ar, and ^{15}N-N_2 determination were pumped from wells into Hungate tubes containing ~150 mg of $ZnCl_2$ (preservative). Tubes were overfilled and sealed bubble free, stored underwater at 5°C, and analyzed for dissolved N_2 and Ar by use of membrane inlet mass spectrometry (Kana et al. 1994) within 2 months of collection. NO_3^- concentrations in samples after storage were within 10% of prestorage concentrations. ^{15}N-N_2 was determined on split samples within 2 weeks of collection, following a modification of the methods of Nielsen (1992). A 4-ml ultra-high-purity He headspace was introduced into the Hungate tubes containing the water samples for ^{15}N-N_2 analysis. Tubes were vortexed for 5 min and allowed to equilibrate submerged in water under refrigeration for 48 h. After equilibration, 1.5 ml of headspace gas was removed; CO_2 was cryogenically removed, and the remaining N_2 was analyzed for ^{15}N by use of a dual inlet Prism IRMS at UVA. Although analytical precision was ~0.3‰, a 10%–80% error (isotopic depletion) in the measured $\delta^{15}N_2$ was observed among duplicate samples as a result of some atmospheric N_2 contamination of the samples during processing.

Isotope incorporation into the sediment organic nitrogen pool (PON) from 0 to 50 cm was determined from cores collected between the injection points and the nearest row of target wells prior to the injection and on day 100 after the injection. No cores were collected during the experiment, to minimize impact on plume transport. Exchangeable DIN was removed from 10-cm core subsections via KCl (2N) extraction, followed by resuspension of sediment in distilled water and centrifugation. The %N, C : N, and ^{15}N of the PON were determined on the acidified and dried sediments simultaneously by use of the Elemental Analyzer–IRMS at UVA.

In situ DNRA and DNF rate analyses—Average peak in situ DNRA and DNF rates for wells 2, 3, and 4 were calculated by use of two methods. The DNRA rate was calculated from the $\delta^{15}NH_4^+$ and $\delta^{15}NO_3^-$ data by use of an isotope-based approach. The total DNF rate was calculated as the sum of the $N_2O \rightarrow N_2$ and net $NO_3^- \rightarrow N_2O$ rates. The $N_2O \rightarrow N_2$ rate was estimated by use of an isotope-based approach similar to that used for the DNRA rate calculation (with $\delta^{15}N_2$ and $\delta^{15}N_2O$ data), whereas the net $NO_3^- \rightarrow N_2O$ rate was estimated from changes in N_2O concentration and plume travel time.

Estimation of DNRA and $N_2O \rightarrow N_2$ rates: isotope-based calculations—In situ estimation of DNRA and $N_2O \rightarrow N_2$ rates were based on the assumption that, within the plume, the peak isotopic enrichment of NH_4^+ or N_2 was a function of the input rates of NH_4^+ or N_2 from labeled and unlabeled sources. The generalized isotope-mixing equation, which related the isotopic enrichment of a product pool to the inputs of labeled and unlabeled sources, was

$$\delta_P = \frac{K_U\delta_U + K_L\delta_L}{K_U + K_L} \tag{1a}$$

where δ_P was the enrichment of the product pool (NH_4^+ or N_2), δ_U was the enrichment of the unlabeled substrate from outside the plume, δ_L was the enrichment of the labeled substrate ($^{15}NO_3^-$ for DNRA, or $^{15}N_2O$ for $N_2O \rightarrow N_2$), K_L was the input rate of labeled substrate into NH_4^+ or N_2, and K_U was the input rate of NH_4^+ or N_2 from unlabeled sources outside the plume. Provided that the NH_4^+ and N_2 pools turn over relatively quickly (faster than the travel time from the injection to the well) and are in near steady state, the gross in situ rate of incorporation of labeled substrate (NO_3^- or N_2O) into the respective reduced products (NH_4^+ or N_2) can be calculated solely from measurements of the isotopic enrichment of the substrates and products and estimates of the production rate of the unlabeled product by setting δ_U equal to zero due to the high plume enrichments, and rearranging Eq. 1 to solve for K_L (Eq. 1b, Fig. 2).

$$K_L = \frac{K_U\delta_P}{\delta_L - \delta_P} \tag{1b}$$

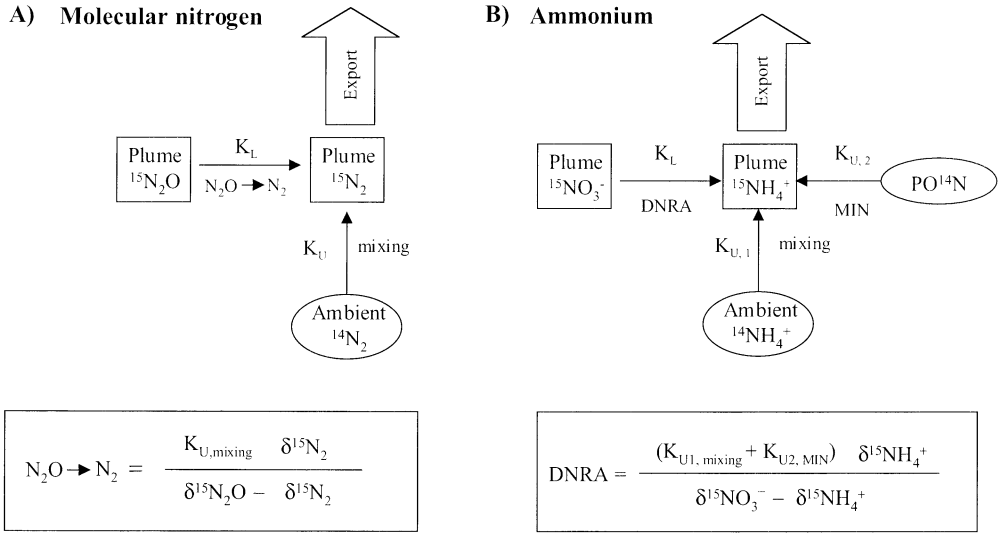

$$N_2O \rightarrow N_2 = \frac{K_{U,\text{mixing}} \quad \delta^{15}N_2}{\delta^{15}N_2O - \delta^{15}N_2}$$

$$\text{DNRA} = \frac{(K_{U1,\text{ mixing}} + K_{U2,\text{ MIN}}) \quad \delta^{15}NH_4^+}{\delta^{15}NO_3^- - \delta^{15}NH_4^+}$$

Fig. 2. Processes effecting isotopic ratios in the N_2 and NH_4^+ pools and derivations of $N_2O \rightarrow N_2$ and DNRA rates.

The δ_L and δ_P values used in the DNRA calculation were the $\delta^{15}NO_3^-$ and $\delta^{15}NH_4^+$ enrichments, respectively. The δ_L and δ_P values used in the $N_2O \rightarrow N_2$ calculation were the $\delta^{15}N_2O$ and $\delta^{15}N_2$ enrichments, respectively. K_U for N_2 was assumed to consist solely of the rate of in-mixing of unlabeled dissolved N_2 from ambient pore water (outside the plume) during plume dilution and calculated as the product of the pore-water N_2 concentration and the pore-water in-mixing rate. This pore-water in-mixing rate was determined from Br^- concentrations according to

$$M = \frac{1}{t}\left(\frac{C_{Br^-,0}}{C_{Br^-,t}} - 1\right) \tag{2}$$

where M was the average rate of ambient pore water mixing into each liter of injectate (liters pore water per liter plume water per day). $C_{Br^-,0}$ and $C_{Br^-,t}$ were the Br^- concentrations of the injectate and of the plume at the target well at the peak of the breakthrough curve, respectively, and t was the time elapsed between injectate release and the appearance of the Br^- peak at the target well. K_U for NH_4^+ consisted of an NH_4^+ in-mixing term ($K_{U,1}$) and a mineralization (MIN) term ($K_{U,2}$; Fig. 2). $K_{U,1}$ was calculated as the product of the in-mixing rate and the pore water NH_4^+ concentration. $K_{U,2}$ was the MIN rate determined in laboratory core incubations of shallow marsh sediments from the site (Tobias et al. 2001*b*). The mineralization rate reported by Tobias et al. (2001*b*) was normalized to a liter of pore water under the assumption of a sediment control volume of 0.075 m^3 (0.75 m^2 of plume area by 10 cm of plume thickness), sediment water content of 56%, and a sediment bulk density of 0.7 gdw cm^{-3} prior to use in the DNRA rate calculation.

Estimation of the net $NO_3^- \rightarrow N_2O$ rate: concentration-based calculations—Equation 1 cannot be used to estimate rates when the mass of the product pool is not near steady state or when the δ_P and δ_L enrichments are equivalent. Therefore, an approach based on changes in N_2O pool size with respect to time was used to estimate the in situ conversion rate of $NO_3^- \rightarrow N_2O$. Because ambient N_2O concentrations were negligible prior to the injection, the average net $NO_3^- \rightarrow N_2O$ rate (excluding N_2O conversion to N_2) for the period between the start of the injection and the appearance of peak Br^- at wells 2, 3, and 4 was calculated according to

$$NO_3^- \rightarrow N_2O = \left(\frac{C_{N_2O,t}}{t}\right) + \left(\frac{MC_{N_2O,t}}{2}\right) \tag{3}$$

where $C_{N_2O,t}$ was the average N_2O concentration in wells 2, 3, and 4 measured at peak Br^- breakthrough, t was the average time elapsed after the injection until peak Br^- breakthrough at each well, and $C_{N_2O,t}/2$ was the mean N_2O concentration in all wells between preinjection and peak Br^- measurements. The net $NO_3^- \rightarrow N_2O$ rate was added to the $N_2O \rightarrow N_2$ rate to yield the total DNF rate (i.e., the gross $NO_3^- \rightarrow N_2O$ rate).

^{15}N-nitrogen mass balance—A total ^{15}N mass balance model for the period encompassing the entire Br^- breakthrough curve (the first 67 d after the injection) was constructed to quantify the storage of N transferred from the NO_3^- pool to each of the identified product pools. The data used in the model originated from three target wells nearest the injection points (wells 2, 3, and 4) and the cores collected for PON characterization (Fig. 1). Each well was assumed to be representative of pore water passing within 25 cm (i.e. one half of the distance to the adjacent well) to a depth of 10 cm (estimated plume thickness). The depth of 10 cm was chosen for the mass balance calculations because hydraulic head data indicated strong vertical (upward) flow, and pumped boreholes were observed to recharge with water primarily from more conductive root-bearing sediments contained within the top 10 cm of the subsurface. For the dissolved pools, each component of the model was determined for each well and then added to estimate the total mass bal-

ance. For sediment PON, data were averaged from duplicate cores and applied to the total sediment volume (75,000 cm^3), which was bounded by the injection points; wells 2, 3, and 4; and the base of the plume.

The ^{15}N mass balance between ^{15}N lost from the NO_3^- pool and ^{15}N incorporated into each of the product pools (NH_4^+, N_2O, N_2, and PON) for the entire experiment was defined by

$$\int C^{15}_{NO_3^-} A\langle u\rangle n \, dt - \sum \int C_i^{15} A\langle u\rangle n \, dt - \Delta C^{15}_{PON} V_{sed} = 0 \quad (4)$$

where $C^{15}_{NO_3^-}$ was the ^{15}N concentration (μM ^{15}N) of the NO_3^- lost from the plume at time t, C_i^{15} was the ^{15}N concentration (μM ^{15}N) incorporated into each of the dissolved product pools ($i = NH_4^+$, N_2O, or N_2) at each sampling time, ΔC^{15}_{PON} was the ^{15}N concentration (μmoles ^{15}N cm^{-3} sediment) incorporated into the sediment PON pool at the end of the study, A was the effective area of each well normal to discharge (500 cm^2 $well^{-1}$), $\langle u\rangle$ was the average groundwater flow velocity between adjacent sampling times, n was sediment porosity (0.56), and V_{sed} was the sediment volume bounded by the target wells and the injection wells. Groundwater flow velocity at the start of the experiment was calculated by dividing the distance between the injection wells and target wells (50 cm) by the travel time required for the peak Br^- arrival at the target well. This initial flow velocity was scaled proportionally through the study according to changes in hydraulic gradient to yield a flow velocity for each sampling time. The concentration of ^{15}N lost from the NO_3^- pool at each sampling time for each well was calculated from concentration measurements of Br^-, NO_3^- and $^{15}NO_3^-$, with use of Eqs. 5, 6, and 7.

$$C^{15}_{NO_3^-,t} = \hat{C}^{15}_{NO_3^-,t} - \overline{C^{15}_{NO_3^-,t}} \quad (5)$$

$$\hat{C}^{15}_{NO_3^-,t} = C_{NO_3^-,0}\left(\frac{C_{Br^-,t}}{C_{Br^-,0}}\right)(R_{NO_3^-} - 0.00365)_t \quad (6)$$

$$\overline{C^{15}_{NO_3^-,t}} = C_{NO_3^-,t}(R_{NO_3^-} - 0.00365)_t \quad (7)$$

where $\overline{C^{15}_{NO_3^-,t}}$ and $\hat{C}^{15}_{NO_3^-,t}$ were the observed and predicted ^{15}N-NO_3^- concentrations at time t, respectively, $C_{NO_3^-,0}$ and $C_{Br^-,0}$ were the nitrate and bromide concentrations in the injection wells immediately after injection of the first slug of injectate, respectively, $C^{15}_{NO_3^-,t}$ and $C_{Br^-,t}$ were the observed nitrate and bromide concentrations at the target well at time t, respectively, and R was the ratio of $^{15}N/^{14}N$ (natural abundance, 0.00365). $\hat{C}^{15}_{NO_3^-,t}$ was the expected ^{15}N-NO_3^- concentration if NO_3^- was a conservative solute.

The concentration of ^{15}N incorporated into each of the reduced dissolved pools (C_i^{15}) was determined for each well at each time from

$$C_i^{15} = (R_i - .00365)C_i \quad (8)$$

where C_i and R_i were the concentration and the $^{15}N/^{14}N$ ratio of the ith product pool, respectively, and i denotes either the NH_4^+, N_2O, or N_2 pools.

The concentration of ^{15}N incorporated into sediment PON (ΔC^{15}_{PON}) during the experiment was calculated from

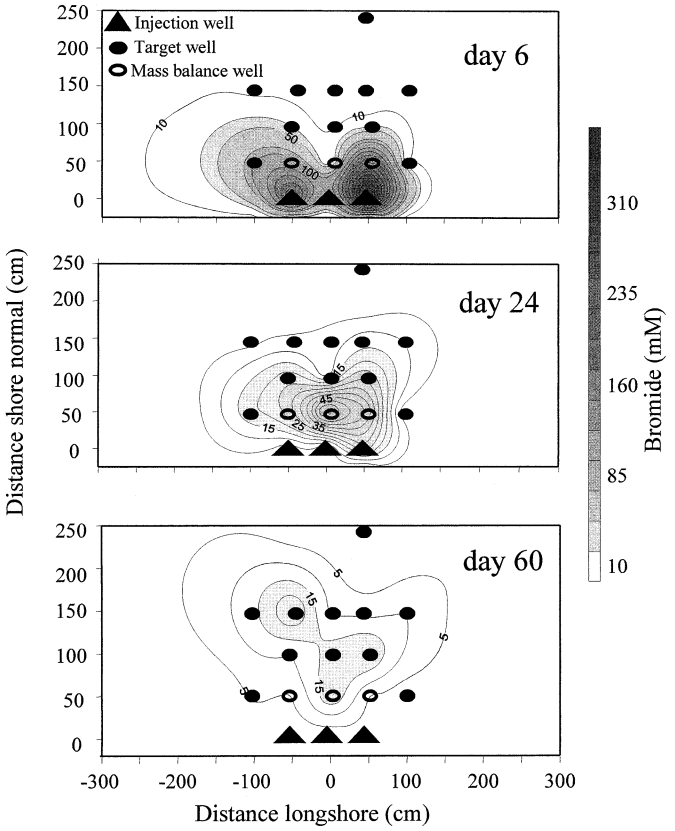

Fig. 3. Bromide contour plot of the plume on days 6, 24, and 60 after the injection. Triangles represent the injection wells. Ovals indicate sampling wells. Open ovals identify wells 2, 3, and 4, from left to right. The upland border is located at a shore normal distance equal to 0.

$$\Delta C^{15}_{PON} = \Delta R_{PON} N_{PON} \rho \quad (9)$$

where ΔR_{PON} was the difference in the sediment $^{15}N/^{14}N$ ratio between preinjection and day 100 of the experiment, and N_{PON} and ρ were the nitrogen content and bulk density (0.7 gdw cm^{-3}) of the sediment, respectively.

Results

Plume transport—Initially, the plume did not migrate as a uniform solute front from the injection wells but instead followed preferential flow paths centered about wells 2 and 4 (Fig. 3). By day 6, the majority of the mass in the plume was located within the sediment volume between the injection points and the first target well fence. By day 24, the two plume centers had merged into one center of mass located near well 3, and by day 60 the plume had migrated to an area of ~5 m^2 with a diffuse center of mass ~1.5 m from the injection wells (Fig. 3). Transport time for the arrival of both peak Br^- and NO_3^- concentrations at the wells used in the mass balance were comparable, which suggests similar physical transport behavior of the two anions. The groundwater flow velocity calculated from peak Br^- breakthrough at wells 2, 3, and 4 on days 11, 17, and 24, respectively, were 4.5, 3, and 2.1 cm d^{-1}, respectively. The hydraulic

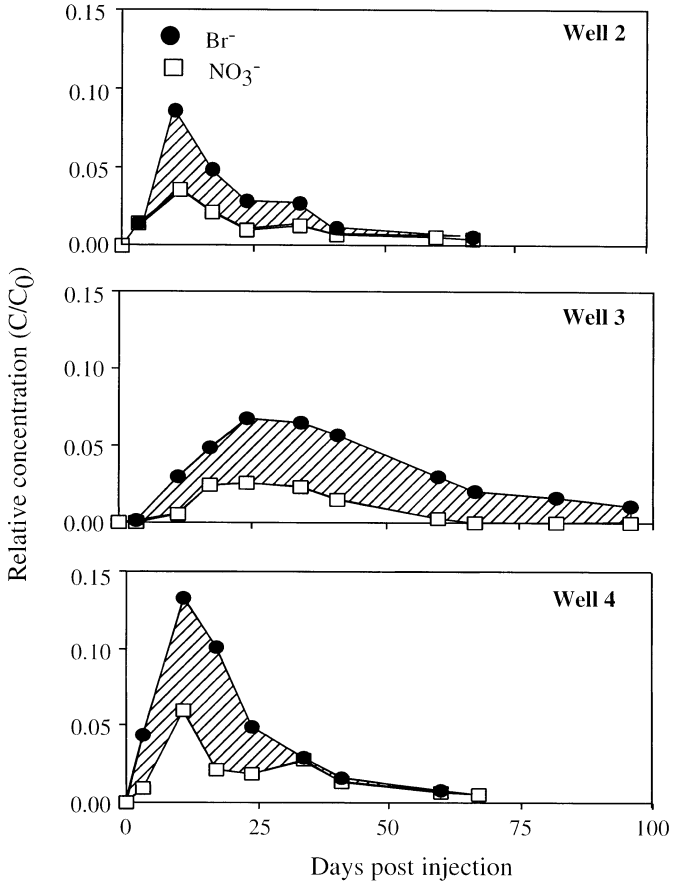

Fig. 4. Breakthrough curves for Br^- and NO_3^-. C/C_0 equals the concentration of Br^- or NO_3^- at the sampling time t, divided by the initial concentration (C_0) in the injection wells. The shaded area represents N-NO_3^- loss during the study.

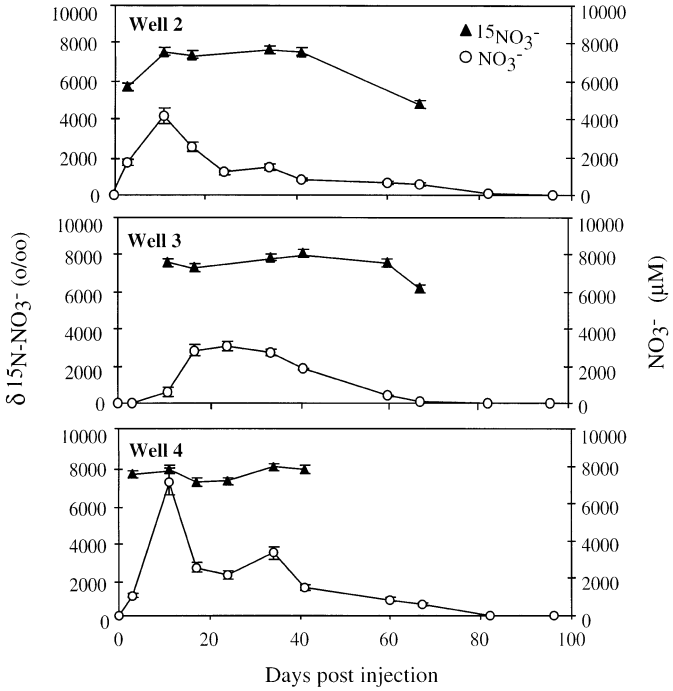

Fig. 5. Nitrate concentrations and isotopic enrichments. Error bars indicate the precision of the isotopic analysis or the range of selected duplicate nitrate samples. All isotopic measurements are expressed as "per mil (‰)" in "δ" notation, where $\delta^{15}N = [(R_{samp} - R_{std})/R_{std}] \times 1000$ and R is the ratio of $^{15}N:^{14}N$ for the sample or air standard. NO_2^- concentrations were measured coincident with NO_3^- analysis and ranged between 0.0 and 3.0 μM at all samplings.

head–adjusted linear velocities showed a linear decrease in the discharge velocity to rates at day 90 that were an average of 50% of the initial velocities for the three wells. Coincident with the decrease in discharge, pore water salinity increased from 0‰ at the start of the experiment to 3–5‰ by day 100. The highest Br^- concentration was encountered in well 4 and indicated that much of plume flowed through the vicinity of well 4. The total Br^- passing through wells 2, 3, and 4 accounted for ~37% of the Br^- released.

Characterization of the N pools—Maximal C/C_o for nitrate encountered at the target wells was 30%–50% of the C/C_o for Br^- at peak values (Fig. 4), and the peak NO_3^- concentrations ranged between 3000 and 7172 μM (Fig. 5). Nitrate loss rates calculated from peak Br^- and NO_3^- concentrations for the three wells averaged 420 μM d^{-1} but ranged between 208 and 645 μM d^{-1}. Approximately 90% of the NO_3^- mass was lost within 67 d, and peak losses in all wells were seen in the first 20–30 d. The isotopic enrichment (δ^{15}N-NO_3^-) for all wells averaged 7528‰ and varied within 10% of the mean for all periods, except the last sampling dates for wells 2 and 3 (Fig. 5). This relatively constant level of enrichment in the NO_3^- pool (equivalent to the δ^{15}N-NO_3^- of the injectate) was indicative of the low ambient NO_3^- concentrations and negligible nitrification rates.

The NH_4^+ concentrations and isotopic enrichments followed a similar temporal pattern in well 3, and to a lesser extent in wells 2 and 4, through the duration of the study (Fig. 6). NH_4^+ concentration ranged between 10.6 and 80.0 μM at the start of the injection and climbed to 56–145 μM during the study. Similar maximal ^{15}N-NH_4^+ enrichments (between days 17 and 34) were observed in all wells and ranged between 2000‰ and 2400‰. The lower peak enrichments (~25%–33% of the ^{15}N enrichment of the NO_3^- pool) reflect primarily isotopic dilution due to the release of NH_4^+ created during the mineralization of unlabeled PON in sediments within the plume. By day 100, both the concentration and the enrichment decreased from peak values to an average of 60% and 20% of their maximum values, respectively.

N_2O concentrations in all wells were undetectable at the start of the experiment and rose to maximal values (200–400 μM) on days coincident with peak Br^- and NO_3^- values (Fig. 7). N_2O concentrations returned to undetectable levels in all wells by day 82. δ^{15}N-N_2O enrichments were constant within the estimate of error at values on a par with the enrichment of the NO_3^- source (7528‰ ± 200‰) for all measurements, which indicates negligible production of, or inmixing of, unlabeled N_2O from outside the plume.

Despite being produced from N_2O during denitrification, neither the dissolved N_2 concentration nor $\delta^{15}N_2$ showed patterns similar to the N_2O pool. Relative to predicted equilib-

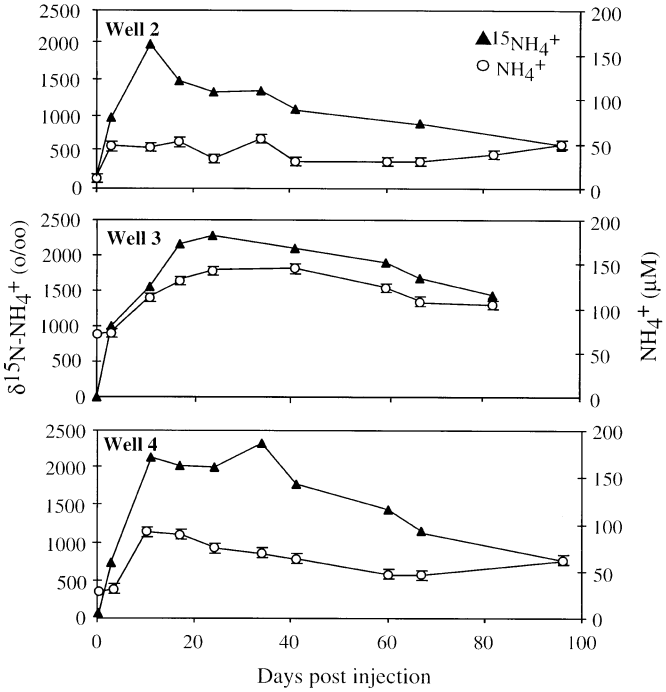

Fig. 6. Ammonium concentrations and isotopic enrichments. Analytical precision for isotope analysis was within 1‰. Error bars for the ammonium concentrations represent the range of selected analytical duplicates.

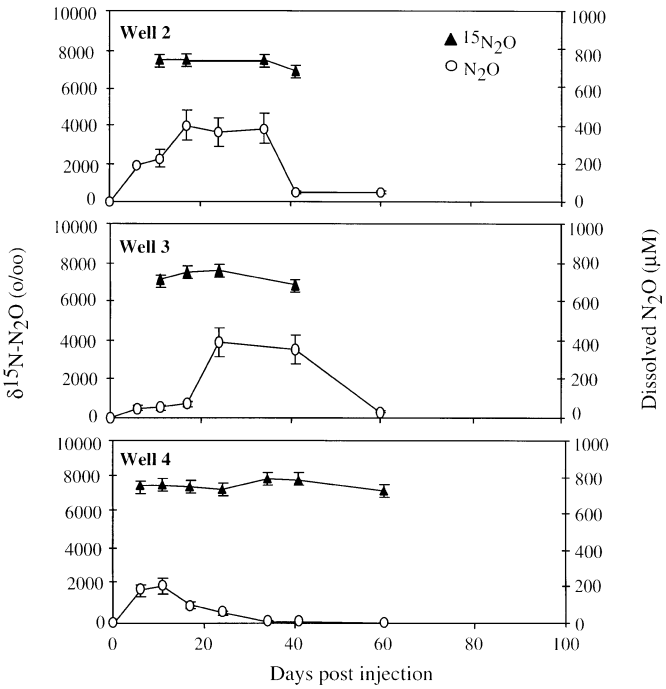

Fig. 7. Dissolved nitrous oxide concentrations and isotopic enrichments. Analytical precision for isotope analyses ranged between 28‰ and 200‰, and the error bars represent the poorest analytical precision observed (200‰). Estimates of error for N_2O concentrations were set at 20% of the mean. This value was derived from replicate standard headspace equilibrations.

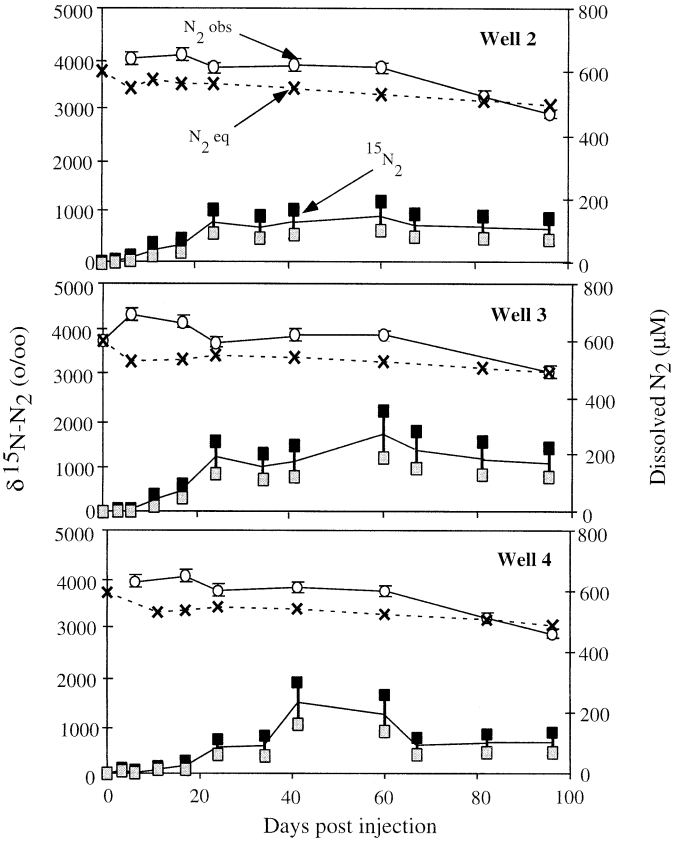

Fig. 8. Observed and predicted equilibrium concentrations for dissolved N_2 and isotopic enrichments. ''X'' denotes predicted N_2 equilibrium concentration based on temperature and salinity (Weiss 1970). Open circles are the observed dissolved N_2 concentrations, with error bars representing an average error of 3% as determined from selected duplicates at all times. Isotopic enrichment of N_2 is reported as a range incorporating the uncertainty in estimating $\delta^{15}N_2$ due to atmospheric contamination during sample processing. Isotopic values on selected duplicates varied between 10% and 80%. The midpoint of the reported range was used in the rate and mass balance calculations.

rium concentrations, there was a maximum dissolved N_2 supersaturation of ~100 μM (Fig. 8). This was equivalent to an increase in dissolved N_2 of 15% above saturation concentrations predicted by temperature and salinity. The dissolved N_2 subsidy disappeared by day 100, when the observed N_2 concentrations were at parity with equilibrium concentrations. The ranges of δ^{15}N-N_2 enrichment increased more slowly than the N_2O and NH_4^+ pools and initially plateaued in all wells at day 34 (Fig. 8). Because of the constant in-mixing of ambient unlabeled N_2, peak δ^{15}N-N_2 enrichments were ~20% of the δ^{15}N-N_2O values. Enrichments declined slightly after day 60 but did not rebound to near preinjection levels within the 100 d.

The dissolved N_2 subsidy was coincident with a deficit in dissolved Ar concentrations relative to predicted equilibrium values (Fig. 9). The observed Ar concentrations fell below the predicted Ar equilibrium (saturation) concentrations predicted by salinity and temperature by day 24 in all wells. The maximum Ar deficit was 77% of the predicted equilib-

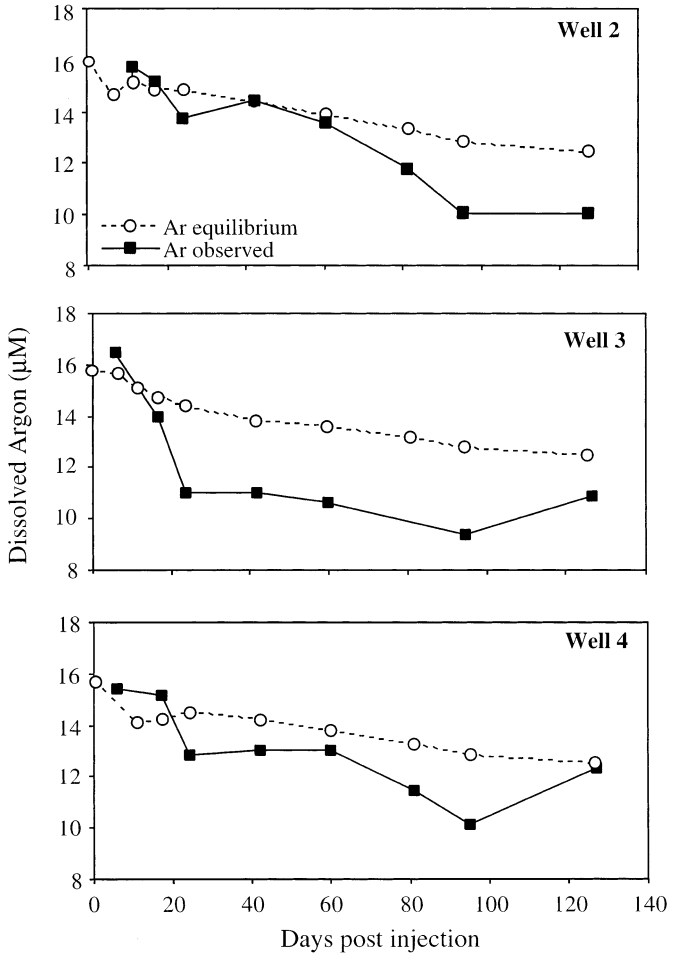

Fig. 9. Predicted and observed dissolved argon concentrations. Errors ranged from 0.01–0.19 μM on the basis of selected duplicates.

rium value (well 3) and trended back toward equilibrium concentrations in wells 3 and 4 near the end of the 100-d period.

Characterization of the sediment PON pool at three depth intervals is given in Table 1. %N and C : N ratios for the three depth intervals ranged from 0.002 to 0.277 and 13.4 to 20.3, respectively. With the exception of %N in the 40–50 cm interval, no difference between preinjection and postinjection values of %N or C : N were detected in excess of the reported ranges. At the end of the study, the isotopic enrichment of the 0–10, 20–30, and 40–50 cm deep sediment PON had increased by 25‰, 6‰, and 5‰, respectively. The ^{15}N mass balance conservatively included only $\delta^{15}N$-PON data from 0–10 cm because it was the only horizon that showed unequivocal isotope incorporation. This horizon was the zone within which we believe the plume was confined and which demonstrated the maximal NO_3^- reducing potential in laboratory studies (Tobias et al. 2001*b*).

In situ DNF and DNRA rate analysis—The net in situ N_2O production rate ($NO_3^- \rightarrow N_2O$) of 201 μM N d^{-1} was calculated from Eq. 3 by use of mean estimates of the peak N_2O concentration (550 μM N), mixing rate (M) of 0.62 d^{-1}, and the average plume travel time (15.3 d). The in situ N_2 production rate ($N_2O \rightarrow N_2$) was calculated from Eq. 1b (Fig. 2) by use of the average peak enrichment of $\delta^{15}N_2O$ (7528‰) and $\delta^{15}N_2$ (1590‰) and the mixing rate of ambient dissolved N_2 into the plume. Under the assumption that ambient pore water was saturated with dissolved N_2 (560 μM N_2), mixing delivered 694 μmoles N as N_2 to the plume each day (K_U). The $N_2O \rightarrow N_2$ rate was therefore 186 μM N d^{-1}. The total DNF rate (defined as the sum of the net $NO_3^- \rightarrow N_2O$ and $N_2O \rightarrow N_2$ rates) was 387 μM N d^{-1}.

The in situ DNRA rate was calculated from the average $\delta^{15}NO_3^-$ enrichment of 7528‰, an average peak $\delta^{15}NH_4^+$ enrichment of 2216‰, the mixing rate of unlabeled NH_4^+ into the plume, and the input rate of unlabeled NH_4^+ from mineralization. Under the assumption that ambient pore water contained 80 μM NH_4^+, pore-water mixing supplied 50 μmoles of unlabeled NH_4^+ to the plume each day (K_{U1}). The resulting in situ DNRA rate of 180 μM N d^{-1} was calculated from Eq. 1b (Fig. 2) after the incorporation of an estimated mineralization rate ($K_{U2,MIN}$) of 216 ng N gdw^{-1} hr^{-1} (Tobias et al. 2001*b*). The estimated mineralization rate used in the calculation was a conservative annual average for the site reported by Tobias et al. (2001*b*) for the previous year.

The sum of the in situ DNRA and DNF rates was 567 μM N d^{-1}. This total rate was within the range of total NO_3^- loss rates calculated independently from NO_3^- and Br^- ratios (208–645 μM N d^{-1}) and ~135% of the average loss rate. DNF and DNRA represent 68% and 32% of the total NO_3^- reduction, respectively, yielding a DNF : DNRA ratio of 2.1. The relative proportions of DNF and DNRA, however, may have been altered by the magnitude of N_2O evasion to the atmosphere. The total DNF rate was based in part on a net $NO_3^- \rightarrow N_2O$ rate estimate that neglected potential N_2O evasion. Although the flux of N_2O to the atmosphere was not directly measured, an upper limit constraint was applied by use of the maximum total NO_3^- loss rate calcu-

Table 1. Characterization of the sediment PON pool prior to the injection and on day 100 (postinjection). Reported values are the average of measurements from duplicate cores at both sampling periods located within 1 m and 50 cm of the upland border for the preinjection and postinjection cores respectively. $\delta^{15}N$-PON is reported in per mil (‰). Average range of duplicates is reported in parentheses.

Depth (cm)	% N		C : N		$\delta^{15}N$	
	Preinjection	Postinjection	Preinjection	Postinjection	Preinjection	Postinjection
0–10	.158 (.096)	.204 (.003)	17.2 (1.5)	17.4 (2.0)	3.2 (0.4)	28.3 (1.1)
20–30	.042 (.038)	.277 (.263)	16.3 (5.6)	13.4 (1.4)	3.8 (0.7)	9.8 (2.6)
40–50	.002 (.006)	.124 (.021)	20.3 (1.6)	19.9 (1.1)	3.7 (1.5)	9.0 (1.3)

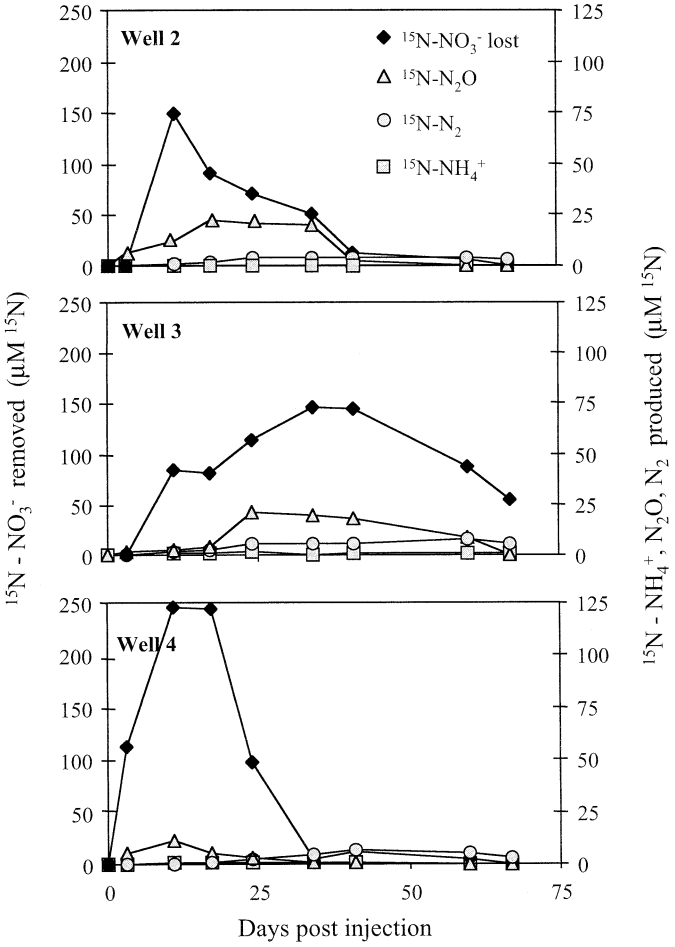

Fig. 10. Summary of ^{15}N lost from NO_3^- and ^{15}N gained in each of the reduced dissolved N pools during the experiment.

lated from NO_3^- bromide $C_o:C_t$ ratios. Under the assumption of a maximum observed total NO_3^- loss rate of 645 μM N d^{-1} and the given $N_2O \rightarrow N_2$ and DNRA rates, the highest potential rate of N_2O export to the atmosphere would be 78 μM N d^{-1}. If this maximum N_2O evasion rate was considered in the rate summary, the DNF rate would increase to 465 uM N d^{-1}. The relative importance of DNF to total NO_3^- reduction would increase from 67% to 72%, and DNRA would decrease to 28% of the total. These values should be regarded as the upper and lower limits of DNF and DNRA, respectively.

^{15}N mass balance—The ^{15}N stored in each of the dissolved reduced N pools was small relative to the amount of ^{15}N lost from the NO_3^- pool for all sample periods (Fig. 10). Storage in these dissolved pools was smallest in the well with the fastest discharge velocity (well 4) and dominated by $^{15}N_2O$ in all wells. The mass balance technique of integrating ^{15}N mass curves is most accurate when the curves for all constituents return to preinjection levels within the mass balance period. As such, this approach may provide the most reasonable estimate of ^{15}N-N_2O storage but could underestimate ^{15}N storage in NH_4^+ and N_2 (Figs. 6–8). Although the $^{15}NH_4^+$ and $^{15}N_2$ mass curves remain elevated above background by the end of the mass balance period, the resulting underestimate in storage was likely to be insignificant because of the small total magnitude of the ^{15}N mass in each of the pools. Total ^{15}N incorporated into PON, NH_4^+, N_2O, and N_2 during the experiment accounted for 22% of the ^{15}N lost from the NO_3^- pool during the mass balance period (Table 2). Despite a more than twofold difference among total ^{15}N recovery among the wells and the low total ^{15}N recovery, the dominant measured sink for ^{15}N in all wells measured was either N_2O (9.6%) or PON (8.1%), followed by N_2 (4.1%) and finally NH_4^+ (0.5%).

Discussion

Low Br^- recovery in the mass balance (37%) relative to Br^- released in the injection wells indicated that two thirds of the plume escaped characterization. Although discrete flow paths between target wells may have transported some of the plume undetected, much of the missing Br^- probably flowed past the wells on the marsh surface. Large vertical hydraulic gradients (Tobias et al. 2001*a*) toward the surface were evidenced by discharging seeps, and Br^- was detected in ponded surface water within the sampling grid. As a result of these vertical gradients and higher conductivity of shallow marsh sediments (Tobias et al. 2000*a*), most of the plume was likely confined to the upper 10 cm of the sediment during discharge. These shallow sediments possessed the highest nitrate reducing potential of any sediment strata underlying the marsh (Tobias et al. 2001*b*) and help account for the high rate of NO_3^- loss from the plume.

The NO_3^- loss rates calculated from the peak of the breakthrough curves, when normalized to marsh area (0.49–1.5 mmoles N m^{-2} hr^{-1}), were higher than denitrification rates reported for NO_3^--rich fresh and salt water marsh sediments (0.071–0.79 mmoles N m^{-2} hr^{-1}; Kaplan et al. 1979; Hattori

Table 2. Balance sheet of ^{15}N loss and gains by well. Bromide and ^{15}N are shown in mmoles and μmoles, respectively. Total ^{15}N masses shown were derived from integrating the curves in Fig. 10 with respect to discharge after cumulative discharge estimation at each sample time using equation 4. The %^{15}N recovered was calculated as the sum of all product pools (NH_4^+, N_2O, N_2, PON) divided by the NO_3^- (loss).

Well	Br^-	NO_3^- (loss)	NH_4^+	N_2O	N_2	PON	Missing ^{15}N	%^{15}N recovered
2	1,282	2,329	9	507	128	283	1,402	40
3	1,161	2,687	20	305	115	283	1,964	27
4	2,841	5,453	28	198	191	283	4,753	13
Total	5,284	10,469	57	1010	434	849	8,119	22

1983; Xue et al. 1999) but were consistent with the broad range (0.8–50 mmoles N m^{-2} hr^{-1}) of observed DNRA rates in natural and nitrate amended estuarine sediments (Koike and Sorenson 1988). For the majority of the 67-d mass balance period, ambient nitrification rates were not sufficient to isotopically dilute the $^{15}NO_3^-$ below the enrichment of the injectate. In contrast, the NH_4^+ pool enrichment in this study was only 25%–33% of the $^{15}NO_3^-$ signal, which indicates that 60%–75% of inputs to the NH_4^+ pool originated from a nonlabeled N source. MIN (the dominant N cycling process in most marshes) rates determined in sediment cores from the site were three times larger than potential DNRA rates determined from nitrate amended sediments (Tobias et al. 2001*b*). These laboratory results were consistent with the observed $\delta^{15}N\text{-}NH_4^+$ in the plume originating from DNRA and being isotopically diluted by a factor of three by mineralization of relatively unlabeled PON.

The dominance of DNF as the favored NO_3^- reduction pathway was in agreement with previous studies (Cooke 1994; Xue et al. 1999) in freshwater wetlands, but the significant portion of total NO_3^- loss reduced via DNRA (30%) has also been demonstrated in anoxic groundwater microcosms (Bengtsson and Annadotter 1989) and in some estuarine sediments (Bonin et al. 1998). Pore-water H_2S concentrations were typically low at the site during high groundwater discharge ($\gg$50 μM) and may have contributed to conditions favoring DNF (Sorenson 1987). However, the DNF : DNRA ratio of 2.2 was approximately the inverse of the DNF : DNRA ratio (0.42) measured in laboratory incubations of the same sediments (Tobias et al. 2001*b*) when H_2S concentrations were similarly low. Instead, we suggest that this discrepancy in DNF : DNRA ratios resulted from the order-of-magnitude higher (millimolar) NO_3^- concentrations observed in the in situ experiment. The resulting higher NO_3^- : dissolved organic carbon ratio not only favored DNF over DNRA (King and Nedwell 1985; Tiedje 1988) but may also have combined with the small groundwater derived dissolved O_2 flux into the marsh sediments (Tobias et al. 2001*b*) to create conditions that lead to the accumulation of N_2O as the principle end product of denitrification (Firestone et al. 1980). Although a tracer experiment that uses millimolar NO_3^- concentrations may at first appear to be extreme, those concentrations are not out of the range of NO_3^- concentrations encountered in highly anthropogenically impacted waters both in the United States and globally. As such, the observed dominance of the $NO_3^- \rightarrow N_2O$ pathway suggests that increases in high NO_3^- delivery to wetlands may be accompanied by a concomitant rise in N_2O emissions from those wetlands to the atmosphere. Regardless of the favored end product of DNF at the high observed NO_3^- concentrations, DNRA reduced 30% of the incoming load and may be even more important in retaining groundwater N when NO_3^- loads are smaller.

Despite the fact that the peak in situ DNRA and DNF rate calculations approximated the peak total NO_3^- loss rates determined from NO_3^- and Br^- ratios, the mass balance of potential products accounted for only ~22% (48% if maximum N_2O evasion is assumed) of the ^{15}N lost from the NO_3^- pool. This inconsistency suggested that either N had a short turnover time in the products of DNRA (NH_4^+) and DNF (N_2O or N_2) and was transferred to pools in the marsh not well characterized in this study or N was quickly exported from the ecosystem. Previous experiments in aquifers and marshes that have attempted to mass balance either labeled or unlabeled products after NO_3^- additions demonstrated higher total N mass recovery. However, these studies were conducted either deeper in the aquifer, where atmospheric exchange was limited and fewer potential biotic N sinks were available (Bates and Spalding 1998), or in marsh enclosures, which restricted potential routes of N export (Xue et al. 1999). Lower recovery in this study was not surprising considering the multiple pools within and unconfined nature of this experiment. We suggest that quick turnover followed by transfer into large, but poorly characterized, marsh N pools was the fate for $^{15}NH_4^+$ produced via DNRA, whereas rapid export to the atmosphere was the fate for the gaseous products of DNF.

Although we estimated that ~30% of the reduced NO_3^- was converted to NH_4^+ via DNRA, the total $^{15}NH_4^+$ inventory during the study accounted for ~1% of the lost $^{15}NO_3^-$. The in situ NH_4^+ production from DNRA in conjunction with the high mineralization rate was nearly balanced by rapid removal of NH_4^+ (Anderson et al. 1997); otherwise, NH_4^+ would have accumulated well in excess of concentrations observed. NH_4^+ removal via nitrification was small, as was evidenced by the constancy of the $\delta^{15}N\text{-}NO_3^-$ signal. Similarly, tidal inundation and flushing of the subsurface during the study period was small (Tobias et al. 2001*a*) and probably was a negligible factor in maintaining the near steady-state NH_4^+ concentrations. In the absence of high in situ nitrification rates or large physical losses of NH_4^+, in-marsh uptake of NH_4^+ must have been nearly equal to NH_4^+ production. Although marsh macrophytes can be considerable sinks for new N (White and Howes 1994; Dai and Weigert 1997), no above-ground macrophyte biomass was actively growing within the area bounded by the injection and target wells used to construct the mass balance and was thus not sampled. However, roots and rhizomes were present but not specifically sampled. Because the ^{15}N in roots and rhizomes were not measured as part of the PON fraction, this pathway could account for a significant ^{15}N sink (White and Howes 1994) that was not measured during the experiment.

Immobilization of $^{15}NH_4^+$ is an alternate mechanism by which labeled NH_4^+ generated from DNRA was removed from the dissolved pool. Under the assumption that ammonium concentrations were sufficiently high to inhibit assimilatory NO_3^- reduction (Bengtsson and Annadotter 1989), Smith et al. (1982) and Tiedje et al. (1981) demonstrated that peak N incorporation into sediment organic nitrogen (immobilization) from a labeled NO_3^- source flows initially either through NO_2^- or NH_4^+. Specifically, high immobilization rates (in pace with ammonification) in marshes have been proposed to explain the co-occurrence of high rates of gross ammonification with steady-state ammonium concentrations (Anderson et al. 1997). However in the present study, DNRA calculations accounted for ~30% of the NO_3^- loss, yet estimates of ^{15}N storage in PON accounted for only 8% of the ^{15}N loss from NO_3^-. Although sediment PON has been shown to be the long-term repository for ^{15}N released into an estuary, this pool is difficult to accurately

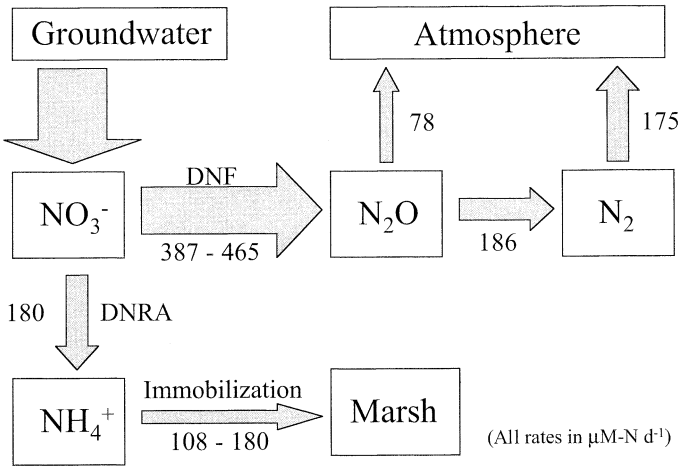

Fig. 11. Rate summary of N loss pathways from groundwater NO_3^-. N_2O evasion (78 μM N d^{-1}) was estimated by the difference under the assumption of the maximum total NO_3^- loss rate (645 μM N d^{-1}) calculated from NO_3^- to Br^- ratios. N_2 evasion was calculated from N_2 mass balance under the assumption of a net rate of N_2 accumulation of 12 μM N d^{-1} calculated from the 15% N_2 supersaturation normalized to travel time. The lower limit of immobilization assumed 18% storage of ^{15}N in PON (i.e., 60% of the DNRA rate). The upper limit of immobilization assumed that the immobilization rate of NH_4^+ kept pace with mineralization (Anderson et al. 1997) and thus exceeded the DNRA rate.

quantify because of the high unlabeled N content and spatially variable ^{15}N distribution (Holmes et al. 2000; Hughes et al. 2000). We suspect that the $PO^{15}N$ inventory in this study may have been underestimated as a result of a conservative depth estimate of labeled sediments. If deeper sediment horizons (>10 cm) that showed potential isotopic enrichment (Table 1) were used in the mass balance calculation, the total ^{15}N storage in PON would increase by a factor of 2.2. This increase would bring the $PO^{15}N$ storage estimate to closer agreement with the estimated proportion of NO_3^- lost via DNRA. Despite uncertainties in $PO^{15}N$ estimates, NH_4^+ itself appears unimportant in long-term storage of allocthonous N but instead serves as an important fast turnover link between DNRA and marsh N demands.

Likewise, DON has been shown to be an important intermediate in some ^{15}N tracer experiments (Bronk et al. 1994) yet in this study would be a relatively minor long-term sink for ^{15}N. DON concentrations determined on select samples were similar to pore-water NH_4^+ concentrations (~100 μM). Although the $DO^{15}N$ was not measured, even if the pool was at maximal enrichment (i.e., equal to the enrichment of the NO_3^- pool), ^{15}N storage in DON could account for no more than 5% of the ^{15}N lost from nitrate in the mass balance.

In contrast to mechanisms of N retention linked to DNRA, much of the N reduced via DNF to N_2O and N_2 was apparently exported from the marsh on relatively short timescales. The in situ DNF rate accounted for ~70% of the NO_3^- loss rate from the plume, yet the storage in the N_2O and N_2 pools collectively accounted for only 14% of the ^{15}N mass lost from the NO_3^- pool. The N_2O concentrations and enrichment (Fig. 7) showed rapid production of labeled N_2O whose source was the added $^{15}NO_3^-$. However, of the total ^{15}N measured in N_2O, on average, <50% was subsequently observed in the N_2 pool of wells 2, 3, and 4. Despite the reported unimportance of N_2O emission after NO_3^- additions to freshwater wetlands (Xue et al. 1999), deficits in the mass balance of N_2O produced from NO_3^- during in situ aquifer C_2H_2 block studies have suggested N_2O loss from shallow aquifers (Bragan et al. 1997). The high N_2O concentrations observed in this experiment were unique among wetland studies and were several orders of magnitude above saturation concentrations. High concentrations, combined with the close proximity of the plume to the atmosphere, suggested that N_2O evasion contributed to the disparity between the high rates of N_2O production and $^{15}N_2O$ storage. When the maximum potential N_2O evasion rate (78 μM d^{-1}) was scaled to the entire 67-d mass balance period for the original volume of the plume, evasion could have accounted for a loss of 2155 μmoles ^{15}N from the N_2O pool. When this value is added back to the $^{15}N_2O$ estimate in the mass balance (Table 2), $^{15}N_2O$ storage would increase by a factor of three and account for one quarter of all the missing ^{15}N in the mass balance.

Similar to the N_2O pool, because only a 15% increase in the dissolved N_2 concentration was noted in the presence of large N_2 isotope incorporation, N_2O conversion to N_2 was probably rapidly followed by N_2 export to the atmosphere. Bates and Spalding (1998) demonstrated that 66% of N_2 produced from denitrification in aquifer microcosms could be explained by increases in the N_2/Ar ratio, whereas the remaining 34% of the N_2 produced was believed to be lost to the atmosphere as a result of N_2 supersaturation. Export of N_2 (and N_2O) to the atmosphere may have been aided by gas stripping. The observed argon undersaturation in the pore water indicated a system subject to active gas stripping, potentially accelerated by bubble formation, which was periodically observed in some pore water samples warmed to ambient air temperature (Chanton et al. 1989). The pattern of Ar undersaturation mimicked that of N_2 supersaturation such that Ar stripping appeared to be closely tied to N_2 export (Figs. 8, 9). Given the Ar deficit, dissolved N_2 concentrations and the solubility ratio of Ar to N (2.5), we estimated that the total amount of N_2 stripped out of the system over the entire study was between 15 and 18 mmoles N. On the basis of this rough calculation, gas stripping of N_2 could account for an additional 5% of the total ^{15}N-NO_3^- lost from all wells, effectively doubling the $^{15}N_2$ storage estimate. Despite this potential increase, the $N_2O \rightarrow N_2$ rate accounted for ~30%–35% of the total rate of NO_3^- reduction, but the $^{15}N_2$ storage would still account for <10% of the mass of ^{15}N lost from the NO_3^- pool. Although some N_2 may have been refixed, we suggest that the remaining missing N in the mass balance was lost as N_2 via evasion.

Evasion rates of gases from aqueous environments are difficult to quantify accurately, and it is beyond the scope of this article to derive a confident estimate of evasion of N_2 from this sedimentary environment. Nevertheless, a first approximation of evasion at the water table–atmosphere interface based on the concentration and gas piston velocity of N_2 was more than sufficient by nearly two orders of magnitude to account for the remaining lack of ^{15}N in the N_2 pool (Hartman and Hammond 1984; Wannikoff 1992). We

suggest that evasion and gas stripping were faster than the estimated N_2 production rate. Therefore, dissolved N_2 concentrations in excess of the observed 15% oversaturation were never detected.

In summary (Fig. 11), up to 90% of the groundwater nitrate load discharging into the Ringfield marsh was reduced rapidly in the upper 10 cm of sediment within the first 50 cm marshward of the upland border. The primary fate of the NO_3^- was denitrification (70% of the total NO_3^- loss rate) with N_2O being the dominant end product (50%–60% of the total DNF rate). Of the 70% of the total groundwater NO_3^- load reduced via DNF (N_2 + N_2O), an estimated 53%–80% was exported to the atmosphere rapidly as a result of evasion and gas stripping. DNRA accounted for 30% of the total NO_3^- loss rate, and the ammonium pool appeared to be a highly active intermediate between DNRA and the ultimate immobilization of new N into PON. The amount of N retained from groundwater NO_3^- loads in the Ringfield marsh was a function of both NO_3^- load and the dominant mechanism of NO_3^- reduction. This study illustrated both the merit of using whole-system isotope releases to determine in situ process rates independent of mass-balance estimates and the need for more extensive multipool sampling in future tracer studies, to achieve better agreement between mass-balance estimates and rate calculations.

References

ALPKEM. 1992. Nitrate/nitrite flow solution methodology. Document 00630. Perstorp Analytical, Inc.

ANDERSON, I. C., C. R. TOBIAS, B. B. NEIKIRK, AND R. L. WETZEL. 1997. Development of a process-based nitrogen mass balance model for a Virginia *Spartina alterniflora* saltmarsh: Implications for net DIN flux. Mar. Ecol. Prog. Ser. **159:** 13–27.

BATES, H. K., AND R. F. SPALDING. 1998. Aquifer denitrification as interpreted from in situ microcosm experiments. J. Environ. Qual. **27:**174–182.

BENGTSSON, G., AND H. ANNADOTTER. 1989. Nitrate reduction in a groundwater microcosm determined by ^{15}N gas chromatography-mass spectrometry. Appl. Environ. Microbiol. **55:** 2861–2870.

BOHLKE, J. K., AND J. M. DENVER. 1995. Combined analysis of groundwater dating, chemical, and isotopic analyses to resolve the history and fate of nitrate contamination in two agricultural watersheds, Atlantic coastal plain, Maryland. Wat. Resour. Res. **31:** 2319–2339.

BOKUNIEWICZ, H. J. 1992. Analytical descriptions of subaqueous groundwater seepage. Estuaries **15:** 458–464.

BONIN, P., P. OMNES, AND A. CHALAMET. 1998. Simultaneous occurrence of denitrification and nitrate ammonification in sediments of the French Mediterranean coast. Hydrobiologia **389:** 169–182.

BOWDEN, W. B. 1986. Nitrification, nitrate reduction, and nitrogen immobilization in a tidal freshwater wetland. Ecology **67:** 88–99.

BRAGAN, R. J., J. L. STARR, AND T. B. PARKIN. 1997. Shallow groundwater denitrification rate measurement by acetylene block. J. Environ. Qual. **26:**1531–1538.

BRONK, D. A., P. M. GLIBERT, AND B. B. WARD. 1994. Nitrogen uptake, dissolved organic nitrogen release, and new production. Science **265:** 1843–1852.

BROOKS, P. D., J. M. STARK, B. B. MCINTEER, AND T. PRESTON. 1989. Diffusion method to prepare soil extracts for automated nitrogen-15 analysis. Soil Sci. Soc. Am. Proc. **53:** 1707–1711.

CAPONE, D. G., AND M. F. BAUTISTA. 1985. A groundwater source of nitrate in nearshore sediments. Nature **313:** 214–216.

CHANTON, J. P., C. S. MARTENS, AND C. A. KELLEY. 1989. Gas transport from methane-saturated, tidal freshwater wetland sediment. Limnol. Oceanogr. **34:** 807–819.

COOKE, J. G. 1994. Nutrient transformations in a natural wetland receiving sewage effluent and the implications for waste treatment. Water Sci. Technol. **29:** 209–217.

DAI, T., AND R. G. WIEGERT. 1997. A field study of photosynthetic capacity and its response to nitrogen fertilization in *Spartina alterniflora*. Estuar. Coast. Shelf Sci. **45:** 273–283.

FETTER, C. W. 1993. Contaminant hydrogeology. Macmillan.

GIBLIN, A. E., AND A. G. GAINES. 1990 Nitrogen inputs to a marine embayment: the importance of groundwater. Biogeochemistry **10:** 309–328.

HARTMAN, B., AND D. E. HAMMOND. 1984. Gas exchange rates across the sediment-water and air-water interfaces in south San Francisco Bay. J. Geophys. Res. **89:** 3593–3603.

HARVEY, J. W., AND W. E. ODUM. 1990. The influence of tidal marshes on upland groundwater discharge to estuaries. Biogeochemistry **10:** 217–236.

HATTORI, A. 1983. Denitrification and dissimilatory nitrate reduction, p. 191–233. *In* D. G. Capone and E. J. Carpenter [eds.], Nitrogen in the marine environment. Academic Press.

HOLMES, R. M., B. J. PETERSON, L. A. DEEGAN, J. E. HUGHES, AND B. FRY. 2000. Nitrogen biogeochemistry in the oligohaline zone of a New England estuary. Ecology **81:** 416–432.

HOWES, B. L., P. K. WEISKEL, D. D. GOEHRINGER, AND J. M. TEAL. 1996. Interception of freshwater and nitrogen transport from uplands to coastal waters: the role of saltmarshes, p. 287–310. *In* K. F. Nordstrom and C. T. Roman [eds.], Estuarine shores: Evolution, environments and human alterations. Wiley.

HUGHES, J. E., L. A. DEEGAN, B. J. PETERSON, R. M. HOLMES, AND B. FRY. 2000. Nitrogen flow through the food web in the oligohaline zone of a New England estuary. Ecology **81:** 433–452.

KANA, T. M., C. DARKANGELO, M. B. HUNT, J. B. OLDHAM, G. E. BENNETT, AND J. C. CORNWELL. 1994. Membrane inlet mass spectrometer for rapid high-precision determination of N_2, O_2, and Ar in environmental water samples. Anal. Chem. **66:** 4166–4170.

KAPLAN, W., I. VALIELA, AND J. M. TEAL. 1979. Denitrification in a salt marsh ecosystem. Limnol. Oceanogr. **24:** 726–734.

KING, D., AND D. B. NEDWELL. 1985. The influence of nitrate concentration upon the end-products of nitrate dissimilation by bacteria in anaerobic salt marsh sediment. FEMS Microbiol. Ecol. **31:** 23–28.

KNOWLES, R. 1990. Acetylene inhibition technique: Development, advantages, and potential problems, p. 151–166. *In* N. P. Revsbech and J. Sorenson [eds.], Denitrification in soil and sediment. Plenum.

KOIKE, I., AND A. HATTORI. 1978. Denitrification and ammonia formation in anaerobic coastal sediments. Appl. Env. Micro. **35:** 278–282.

———, AND J. SORENSON. 1988. Nitrate reduction and denitrification in marine sediments, p. 251–270. *In* T. Blackburn and J. Sorenson [eds.], Nitrogen cycling in the coastal marine environments. Wiley.

KRAYNOV, S. R., G. A. SOLOMIN, AND V. P. ZAKUTIN. 1992. Redox conditions for nitrogen-compound transformations in groundwater. Geochem. Int. **6:** 822–831.

NIELSEN, L. P. 1992. Denitrification in sediment determined from nitrogen isotope pairing. FEMS Microbiol. Ecol. **86:** 357–362.

NOWICKI, B. L., E. REQUINTA, D. VAN KEUREN, AND J. PORTNOY.

1999. The role of sediment denitrification in reducing groundwater-derived nitrate inputs to Nauset Marsh Estuary, Cape Cod, Massachusetts. Estuaries **22:** 245–259.

PETERSON, B. J., M. BAHR, AND G. W. KLING. 1997. A tracer investigation of nitrogen cycling in a pristine tundra river. Can. J. Fish Aquat. Sci. **54:** 2361–2367.

PORTNOY, J. W., B. L. NOWICKI, C. T. ROMAN, AND D. W. URISH. 1997. The discharge of nitrate-contaminated groundwater from a developed shoreline to a marsh-fringed estuary. Water Resour. Res. **34:** 11, 3095–3104.

REAY, W. G., D. L. GALLAGHER, AND G. M. SIMMONS. 1993. Sediment-water column nutrient exchanges in Southern Chesapeake Bay nearshore environments. Virginia Water Resour. Bull. **181:** all.

REILLY, T. E., AND A. S. GOODMAN. 1985. Quantitative analysis of saltwater-freshwater relationships in groundwater systems—a historical perspective. J. Hydrol. **80:** 125–160.

SMITH, C. J., R. D. DELAUNE, AND W. H. PATRICK, JR. 1982. Nitrate reduction in *Spartina alterniflora* marsh soil. Soil Sci. Soc. Am. J. **46:** 748–750.

SOLORZANO, L. 1969. Determination of ammonia in natural waters by the phenolhypochlorite method. Limnol. Oceanogr. **14:** 799–801.

SORENSON, J. 1987. Nitrate reduction in marine sediment: Pathways and interactions with iron and sulfur cycling. Geomicrobiol. J. **5:** 401–422

TANK, J. L., AND OTHERS. 2000. Analysis of nitrogen cycling in a forest stream during autumn using a ^{15}N tracer. Limnol. Oceanogr. **45:** 1013–1029.

TIEDJE, J. M. 1988. Ecology of denitrification and dissimilatory nitrate reduction to ammonium, p. 179–224. *In* A. Zehnder [ed.], Biology of anaerobic organisms. Wiley.

———, J. SORENSON, AND Y. L. CHANG. 1981. Assimilatory and dissimilatory nitrate reduction: Perspectives and methodology for simultaneous measurements of several nitrogen cycle processes, p. 331–342. *In* F. E. Clark and T Rosswall [eds.], Terrestrial nitrogen cycles. Ecology Bulletin 33. Swedish Natural Science Research Council, Stockholm.

TOBIAS, C. R., J. W. HARVEY, AND I. C. ANDERSON. 2001*a*. Quantifying groundwater discharge through riparian wetlands to estuaries: Seasonal variability, methods comparison, and implications for wetland-estuary exchange. Limnol. Oceanogr. **46:** 604–615.

———, I. C. ANDERSON, AND E. A. CANUEL. 2001*b*. Nitrogen cycling through a fringing marsh—aquifer ecotone. Mar. Ecol. Prog. Ser. **210:** 25–39.

VALIELA, I., AND OTHERS. 1992. Couplings of watersheds and coastal waters: Sources and consequences of nutrient enrichment in Waquoit Bay, Massachusetts. Estuaries **15:** 443–457.

———, AND J. M. TEAL. 1979. Nitrogen budget for a salt marsh ecosystem. Nature **280:** 652–655.

WANNIKOFF, R. 1992. Relationship between wind speed and gas exchange over the ocean. J. Geophys. Res. **97:** 7373–7382.

WEISS, R. F., AND B. A. PRICE. 1980. Nitrous oxide solubility in water and seawater. Mar. Chem. **8:** 347–359.

WHITE, D. S., AND B. L. HOWES. 1994. Long term ^{15}N-nitrogen retention in the vegetated sediments of a New England salt marsh. Limnol. Oceanogr. **39:** 1878–1892.

XUE, Y., D. A. KOVACIC, M. B. DAVID, L. E. GENTRY, R. L. MULVANEY, AND C. W. LINDAU. 1999. *In situ* measurements of denitrification in constructed wetlands. J. Environ. Qual. **28:** 263–269.

Received: 30 December 2000
Accepted: 30 July 2001
Amended: 7 August 2001